



Apatite (U-Th)/He Thermochronology Evidence for Two Cenozoic Denudation Events in the Eastern Part of the Sulu Orogenic Belt.

Li Xu, Wu Lin, Marc Jolivet, Chang'An Li, Haijin Liu

► To cite this version:

Li Xu, Wu Lin, Marc Jolivet, Chang'An Li, Haijin Liu. Apatite (U-Th)/He Thermochronology Evidence for Two Cenozoic Denudation Events in the Eastern Part of the Sulu Orogenic Belt.. Earth Science, 2022, 47 (4), 16 p. 10.3799/dqkx.2019.000 . insu-03601008

HAL Id: insu-03601008

<https://insu.hal.science/insu-03601008>

Submitted on 8 Mar 2022

HAL is a multi-disciplinary open access archive for the deposit and dissemination of scientific research documents, whether they are published or not. The documents may come from teaching and research institutions in France or abroad, or from public or private research centers.

L'archive ouverte pluridisciplinaire **HAL**, est destinée au dépôt et à la diffusion de documents scientifiques de niveau recherche, publiés ou non, émanant des établissements d'enseignement et de recherche français ou étrangers, des laboratoires publics ou privés.

1苏鲁造山带东段新生代两阶段剥露事件的磷灰石(U-Th)/He热年代学 2证据

3林旭^{1,2,4}, 吴林², Jolivet Marc³, 李长安⁴, 刘海金⁵

41.三峡大学, 宜昌 276005

52.中国科学院地质与地球物理研究所, 北京 100029

63.法国雷恩第一大学, 雷恩

74.中国地质大学(武汉), 武汉 430074

85.东华理工大学, 南昌 330013

9

10摘要: 苏鲁造山带位于华北和华南板块之间, 是中国东部最显著的陆内造山带之一, 约束其新
11生代剥露过程对于理解中国东部盆山格局分布及其动力学机制具有重要意义。低温热年代学方
12法由于封闭温度较低, 能更准确地约束上地壳地质体的剥露过程。文中利用磷灰石(U-Th)/He
13方法, 对苏鲁造山带东部的多福山和锯齿山开展研究。磷灰石(U-Th)/He 年龄-高程和热历史模
14拟结果显示, 多福山和锯齿山在早-中始新世(54-43 Ma)和渐新世(35-27 Ma)发生剥露。这与苏
15鲁造山带西段的剥露时间同步。结合区域内已报道的研究结果, 表明中国东部造山带受太平洋
16板块向欧亚大陆俯冲的影响, 在早新生代出现广泛的阶段性剥露过程, 从而奠定了中国东部的
17盆山分布格局。

18关键词: 苏鲁造山带, 磷灰石, 隆升, (U-Th)/He 热年代学

19Apatite (U-Th)/He thermochronology evidence for two Cenozoic denudation

20events in the eastern part of the Sulu orogenic belt

21Lin Xu^{1,2,4}, Wu Lin², Jolivet Marc³, Li Chang'an⁴, Liu Haijin⁵

221. China Three Gorges University, Yichang 276005, China

232. Institute of Geology and Geophysics, Chinese Academy of Sciences, Beijing 100029, China

243. Univ Rennes, CNRS, Géosciences Rennes, UMR6118, CNRS – F-35000 Rennes, France

254. China University of Geosciences, Wuhan 430074, China

265. East China Institute of Technology, Nanchang 330013, China

27

28Abstract: The Sulu orogenic belt, located between the North China and South China plates, is one of
29the most prominent intracontinental Cenozoic orogenic belt in eastern China. Therefore, the
30denudation history of the Sulu orogenic belt provides significant insight into the basins-ranges
31evolution in eastern China and their driving geodynamic mechanism. The low closure temperature (ca.

1¹基金项目: 国家自然科学基金(41972212); 湖南省自然科学基金项目(2019JJ40198)

2 第一作者简介: 林旭(1984-), 男, 副教授, 主要从事造山带隆升和中国大河演化研究。E-mail:

3 hanwiji-life@163.com

4 通讯作者: 李长安(1956-), 男, 教授, 主要从事长江演化与第四纪地质学的科研与教学工作。E-mail:

5 chanli@cug.edu.cn

3270°C) of the apatite (U-Th)/He systema allows accurate constraint of the cooling processes of
33 geological bodies in the upper crust. In this study, the apatite (U-Th)/He method was used to analyze
34 the exhumation time of rocks on the Duofu and Juchi Mountains, eastern Sulu orogenic belt. The
35 apatite (U-Th)/He age-elevation relationship and thermal history simulation results showed that the
36 exhumation occurred in the Early-Middle Eocene (54-43 Ma) and Oligocene (35-27 Ma) for the
37 Duofu and Juchi Mountains, respectively. These cooling episodes were synchronous to the
38 exhumation of the western part of the Sulu orogenic belt. Combined with the results previously
39 available in the region, it is showed that the geodynamics of eastern China was influenced by the
40 Pacific plate subduction underneath eastern Asia. Extensive exhumation occurred in the early
41 Cenozoic, which established the basin-mountain distribution pattern during this time.

42 **Key Words:** Sulu orogenic belt, Uplift, Apatite (U-Th)/He thermochronology

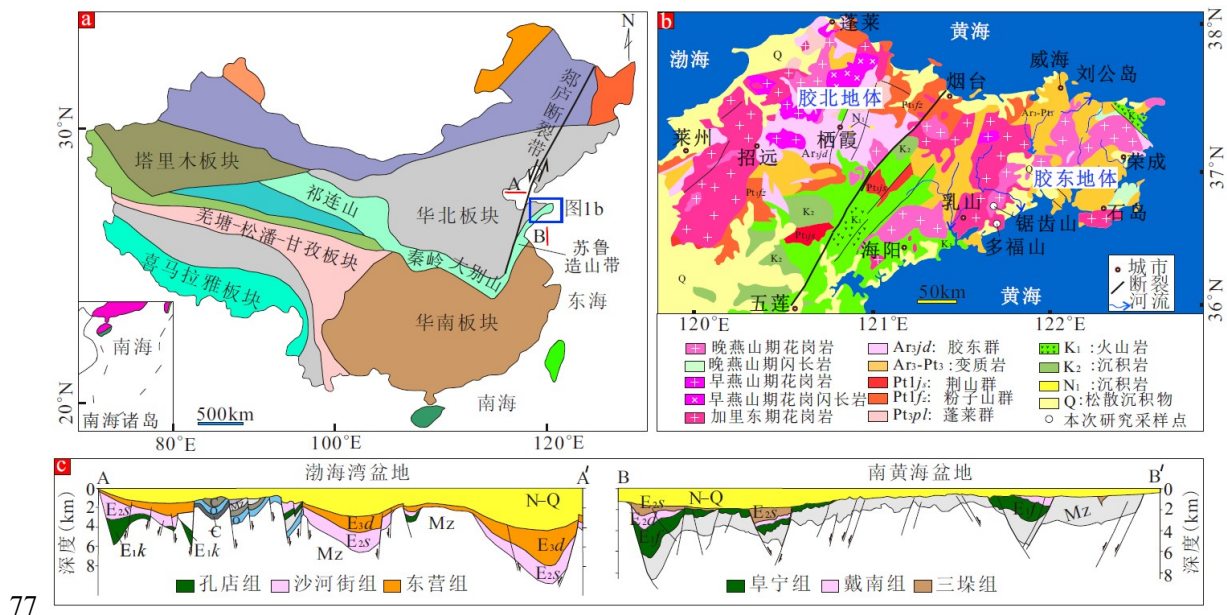
43

44 秦岭-大别-苏鲁造山带是华北克拉通与华南板块在中三叠世发生陆-陆碰撞形成的陆内造山
45 带(Wu and Zheng, 2013; Li et al., 2019, 图 1a)。它不仅是世界上出露规模最大、保存最好的超
46 高压变质地体之一，而且也是陆-陆碰撞之后在超高压岩石折返和剥露过程中岩浆活动最为强烈
47 的地区之一(Zheng et al., 2008; 朱日祥等, 2020)。因此是研究陆-陆碰撞引起岩体剥露过程的理
48 想靶区(Hu et al., 2006; Wu et al., 2016; Ding et al., 2021)。对其剥露(构造过程、地表侵蚀等作用
49 造成地表或地下某一点物质的垂直移离)时间的限定，有助于理解中国中东部陆内造山带的演
50 化过程及其动力学机制(周祖翼, 2015)。前人曾对秦岭、大别山和苏鲁造山带中、新生代期间
51 的剥露历史开展了大量研究，集中在其西部(陈安定等, 2004; 胡圣标等, 2005; Hu et al., 2006; Liu
52 et al., 2009; Siebel et al., 2009; Zhang et al., 2020; Ding et al., 2021)和东段的北部(Wu et al., 2016,
53 2017; Zhao et al., 2018)。而苏鲁造山带南部的数据相对匮乏，因此整个苏鲁造山带在新生代何
54 时开始整体剥露一直没有得到很好的厘定，同时在空间上苏鲁造山带东段南北的剥露时间是否
55 同步也尚不可知。

56 磷灰石(U-Th)/He 年龄体系具有已知最低的放射性同位素封闭温度(70°C)(Jolivet et al.,
57 2010; Shen et al., 2016; 张炜斌等, 2016; Yang et al., 2016; Wu et al., 2021)，近年来已被广泛应用
58 于造山带剥露研究(Wu et al., 2017, 2020; Liu-Zeng et al., 2018; 林旭和刘静, 2019; Yu et al., 2019;
59 Ge et al., 2020; Cao et al., 2021; Ding et al., 2021)。因而，为了解答上述问题，我们对苏鲁造山
60 带东段胶东半岛南部的锯齿山和多福山开展了基岩磷灰石(U-Th)/He 年龄分析，并与周缘已有
61 的低温热年代学结果进行了对比分析，获得了区域内新生代早期两阶段剥露事件新证据，这可
62 为更好的认识中国东部盆山分布格局重建提供重要参考。

631 地质背景

64 苏鲁造山带位于中国中东部，宽约 180 km，长约 750 km，整体呈北东-南西向展布，通常
 65 被认为是大别造山带的延伸，但被北东向的郯庐断裂带大幅度左旋错断(许立青等，2016; Wu e
 66 al., 2016)。苏鲁造山带是中三叠世华北克拉通与华南板块之间的陆陆碰撞造山的产物(Li et al.,
 67 2019)，也是世界范围内出露最好的超高压变质地体之一，已成为研究陆-陆碰撞造山过程的天
 68 然实验室(Liu et al., 2009; Wu and Zheng, 2013; Wu et al., 2017)。苏鲁造山带东段现今地表出露
 69 的岩石类型以新元古代花岗片麻岩和中生代岩浆岩为主(Zheng, 2008)。苏鲁造山带最东端即胶
 70 东半岛，该区以五莲-烟台断裂为界(图 1b)，在构造上可分为胶北地体和胶东地体(山东区域地
 71 质志, 1991)。其中胶北地体具有华北克拉通的属性，而胶东地体具有苏鲁超高压的属性，中生
 72 代岩浆广泛侵入其中。前人的锆石 U-Pb 年龄(Tang et al., 2008; Yang and Santosh, 2014)表明该区
 73 的中生代岩浆岩主要形成于晚三叠纪(225-205 Ma)，晚侏罗纪(160-150 Ma)和早白垩纪(130-110
 74 Ma)。南黄海盆地(Zhu et al., 2020)和渤海湾盆地(Tan et al., 2018; Sun et al., 2020)是位于苏鲁造
 75 山带南北两侧的中-新生代沉积盆地，保存其内的碎屑沉积地层出现角度不整合指示区域内在
 76 新生代期间发生了两期构造事件(图 1c)，分别发生在始新世和渐新世。



78 图 1 苏鲁造山带位置图(a), (b)胶东半岛地质简图(修改自中国 1:250 万地质图); (c) A-A' 和 B-B'
 79 代表渤海湾盆地和南黄海盆地地震反射剖面

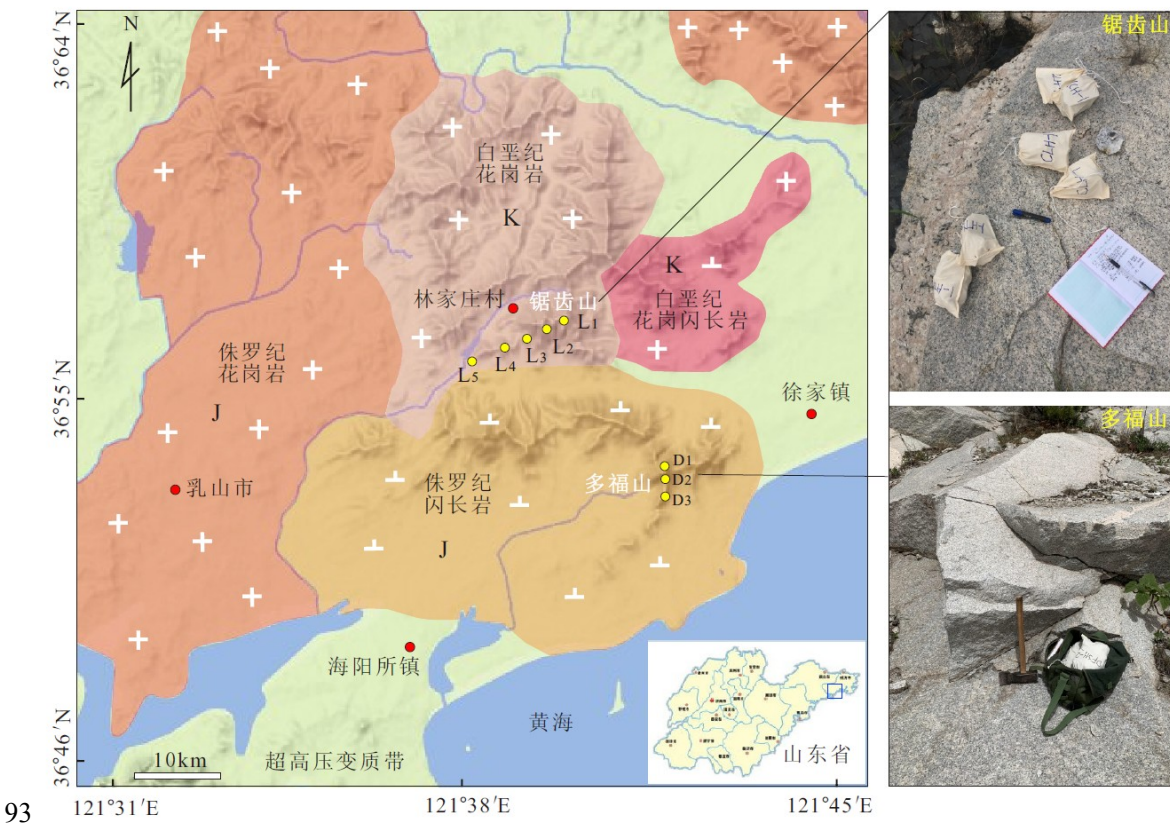
80 Fig. 1 Location map of Sulu orogenic belt, (b) Geological map of Jiaodong Peninsula (Modified from
 81 China 1:2.5 million geological map); (c) A-A' and B-B' represent seismic reflection profiles of the
 82 Bohai Bay Basin and the South Yellow Sea Basin

842.1 样品采集

85 为了**更好**约束胶东地体南部的剥蚀历史, 本文的磷灰石(U-Th)/He 热年代学研究采用年龄-高
86程法来进行样品采集。我们在胶东地体南部的锯齿山和多福山共采集年代学样品 8 件。其中样
87品 D1-D3 采自多福山中粗粒闪长岩(锆石 U-Pb 年龄 161 Ma, 郭敬辉等, 2005, 表 1); 样品 L1-L5
88采自锯齿山中粗粒二长黑云母花岗岩(锆石 U-Pb 年龄 119.6-114.2 Ma, 李增达等, 2018)。多福山
89样品采集高程为 126-350m, 样品采集的高差为 100 m; 锯齿山样品采集高程为 65-383 m, 样品
90采集高差为 50-100 m, [采样点可见图 2](#)。

91 表 1 采样位置、高程、岩性数据表
92 Table 1 Sample location, elevation, petrology

样品号	海拔(m)	经度	纬度	岩性
D1	350	36°53'03"	121°43'12	闪长岩
		"	"	
D2	253	36°52'59"	121°43'06	闪长岩
		"	"	
D3	126	36°52'51"	121°43'02	闪长岩
		"	"	
L1	383	36°56'14"	121°40'09	花岗岩
		"	"	
L2	293	36°55'53"	121°40'08	花岗岩
		"	"	
L3	179	36°55'47"	121°39'53	花岗岩
		"	"	
L4	123	36°55'32"	121°39'40	花岗岩
		"	"	
L5	65	36°55'22"	121°39'20	花岗岩
		"	"	



94 图 2 多福山和锯齿山地质图(修改自乳山 1:20 万区域地质图)和样品采集点分布图

95 Fig. 2 Geological map of Duofu and Juchi Mountains(Modified from Rushan 1:200,000 regional
96 geological map) and distribution map of sample collection points

97

98 2.2 实验方法

99 磷灰石(U-Th)/He 测试工作在中国科学院地质与地球物理研究所 $^{40}\text{Ar}/^{39}\text{Ar}$ 和(U-Th)/He 年代
100 学实验室完成。主要实验流程是, 首先经过标准的岩石破碎和重液分离程序, 在显微镜下优先
101 选择宽度超过 $60 \mu\text{m}$ 的晶粒, 确保颗粒中没有可见的包裹体和内部裂隙, 对 2-5 颗自形磷灰石
102 进行精确测量, 以实现 α 校准因子(F_α)的计算。然后将每个颗粒包裹在 $1\text{mm} \times 1\text{mm}$ 铂(Pt)胶囊
103 中, 并将其装入无氧铜盘中。使用 Alphachron MK II (Australian Scientific Instrument Pty
104 Limited) 仪器进行氦(He)含量提取。之后将铂包裹磷灰石颗粒转移到 Savillex PFA 瓶中, 加入已
105 知浓度的 $^{230}\text{Th} - ^{235}\text{U}$ 溶液。所有加标溶液在 Thermo Fisher X-II 电感耦合等离子体质谱(ICP-MS)
106 上测量。最后年龄计算由基于 Java 程序的 Helioplot 软件实现(Vermeesch, 2010), 并按照
107 Gautheron 等(2009)的程序对 α 离子射出效应(F_α)进行校正。MK-1 磷灰石作为参考标准来验证
108 实验分析精度(Wu et al., 2019)。具体实验流程可参考 Wu et al. (2016, 2019)。

109 磷灰石的(U-Th)/He 测试结果不仅可以提供样品的热年代学年龄值, 通过热历史模拟还可
110 以反演样品经历的热演化史。因此, 本文利用 HeFTy 软件(v1. 9. 3, Ketcham, 2005) 对样品进行

111热历史反演，**主要过程是**：1) 采用辐射损伤累积和退火模型(RDAAM) (Flowers et al., 2009); 2)
112反演时设置 AHe 封闭温度为 70°C，地表温度为 20°C，初始冷却温度范围在 200°C-140°C，输
113入所有测量 AHe 年龄的加权平均值，晶粒半径(Rs)，铀(U)、钍(Th); 3) 每个样品颗粒模拟过
114程一直进行到获得 100 次以上的“好”的拟合路线(拟合度(GOF)≥0.5)为止。

115

1163 实验结果

1173.1 单颗粒年龄结果

118 本次研究使用的磷灰石(U-Th)/He 数据如表 2 所示。多福山样品 D1 的(U-Th)/He 年龄为
 119 48.9 ± 3.6 - 44.2 ± 3.2 Ma, 平均年龄为 45.9 ± 3.8 Ma。样品 D2 的年龄为 53.1 ± 3.8 - 38.6 ± 2.9 Ma, 平
 120 均年龄为 44.8 ± 3.3 Ma。样品 D3 的年龄为 54.9 ± 4.0 - 36.8 ± 2.7 Ma, 平均年龄为 42.6 ± 3.7 Ma。锯
 121 齿山样品 L1 的(U-Th)/He 年龄为 64.5 ± 3.8 - 47.3 ± 2.8 Ma, 平均年龄为 54.0 ± 3.7 Ma。样品 L2 的年
 122 龄为 57.9 ± 3.4 - 44.9 ± 2.7 Ma, 平均年龄为 51.0 ± 3.5 Ma。样品 L3 的年龄为 47.6 ± 2.8 - 41.1 ± 2.4

123Ma, 样品号 L4 的年龄为 39.9 ± 2.4 Ma, 初期年龄 31.5 ± 1.9 Ma, 平均年龄为 34.7 ± 3.0 Ma。样品 L5 的年龄为 27.9 ± 2.8 Ma, 平均年龄为 27.3 ± 2.0 Ma。此外, AHe 年龄的准

125 确保必须考虑晶体尺寸(半径, R_s)和有效U浓度($eU = U + 0.235U_{Th}$)的影响, 因为这两个参数

126对 He⁴的微影响不可忽视的影响(Reiners and Farley, 2001), 我们通过 AHe 年龄 45.8 ± 3.3a) 和

D2-A1 3.31 50.3 2 1.2 2.3 38.77 1.98 0.73 53.11 3.8
 127eU(图3b)二维散点图来辨别其是否具有相关性。结果表明,无论是多福山还是锯齿山的样品,

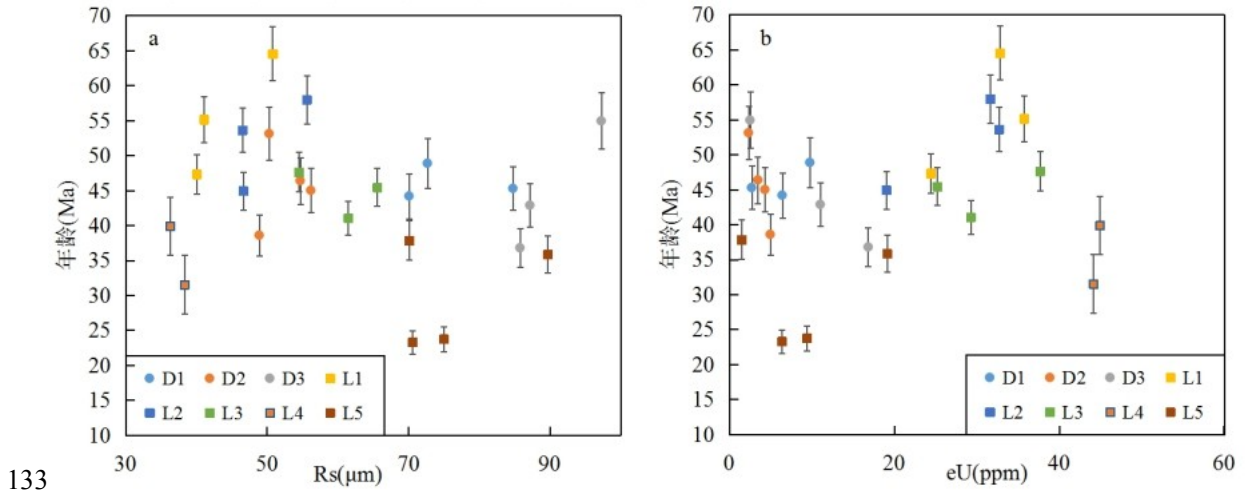
128 其 AHe 年龄与 RS 和 eU 不存在正相关关系，说明晶粒尺寸或辐射损伤并未对 AHe 年龄产生影响

129响(Reimers and Farley, 2001; Shuster et al., 2006)。平均年龄 44.8 岁，3.3 岁。

Table D3 (N_ATh)/He analytical results for samples 130-131 from the vertical transect in the Dushan and Jiaochi Shan.

平均年龄 42.6 3.7

平均年龄								42.6	3.7	
L1-A1	1.83	41.1	14.2	91.7	35.7	35.84	1.16	0.65	55.14	3.28
L1-A4	3.49	50.8	13.3	83.1	32.8	46.02	1.49	0.713	64.54	3.84
L1-A5	1.54	40	10.3	60.2	24.5	30.52	1.01	0.645	47.32	2.84
平均年龄								54.0	3.7	
L2-A1	2.58	46.6	8	46.9	19	31	1.02	0.69	44.93	2.69
L2-A2	2.54	46.5	12.7	85.2	32.7	36.9	1.19	0.688	53.63	3.19
L2-A4	4.2	55.6	12.6	80.8	31.6	42.65	1.37	0.736	57.95	3.44
平均年龄								51.0	3.5	
L3-A1	5.99	61.5	11.6	75.2	29.3	31.17	1	0.759	41.07	2.44
L3-A2	7.54	65.6	10.9	61.1	25.2	35.21	1.15	0.775	45.43	2.71
L3-A3	4.06	54.5	16.1	91.6	37.7	34.86	1.13	0.732	47.62	2.84
平均年龄								44.4	3.1	
L4-A1	1.52	38.3	17.1	115.3	44.2	19.76	0.65	0.627	31.52	1.89
L4-A2	1.31	36.3	18	114.6	44.9	24.33	0.79	0.61	39.89	2.38
平均年龄								34.7	3.0	
L5-A1	9.33	70.6	5.8	2.6	6.4	18.74	0.96	0.805	23.28	1.67
L5-A2	7.93	70.1	1.4	0.5	1.5	30.44	1.65	0.804	37.86	2.79
L5-A3	10.86	75	9.2	1.2	9.4	19.42	1.05	0.818	23.74	1.75
L5-A4	16.89	89.7	18.5	2.6	19.1	30.35	1.64	0.847	35.83	2.64
平均年龄								27.3	2.0	



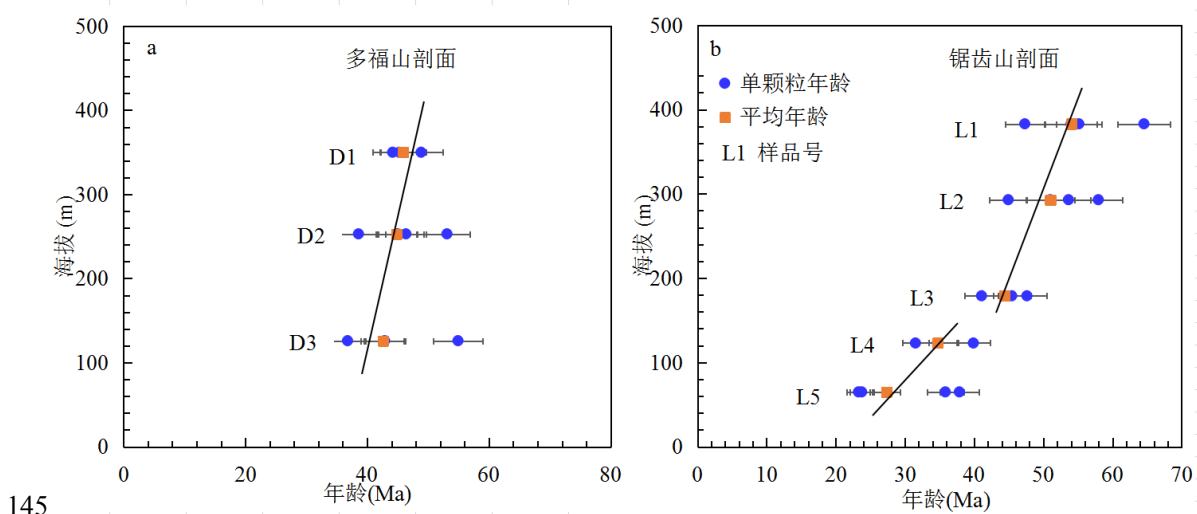
134 图 3 磷灰石 He 年龄和颗粒半径(Rs)(a)、有效铀浓度(eU)(b)二维散点图

135 Fig. 3 Scatter diagram of apatite He age, grain radius (Rs)(a) and effective uranium concentration (Eu)
136(b)

137

138 3.2 年龄高程剖面

139 本次所有样品测试年龄远小于其岩体结晶基底锆石 U-Pb 年龄，表明磷灰石(U-Th)/He 年龄
140 是后期因剥露去顶通过部分保存带(PRZ)的冷却年龄。多福山剖面底部 D3 样品平均年龄为
141 42.6 ± 3.7 Ma(图 4a)，向上 D1 样品的平均年龄递增到 45.9 ± 3.8 Ma，锯齿山底部样品 L5 的平均
142 年龄为 27.3 ± 2.0 Ma(图 4b)，向上样品 L4 的平均年龄为 34.7 ± 3.0 Ma；样品 L3 的平均年龄为
143 44.4 ± 3.1 Ma，向上样品 L1 的平均年龄为 54.0 ± 3.7 Ma。总体来看，两个剖面的实测磷灰石(U-
144 Th)/He 年龄符合各自的年龄-高程图，即年龄自底部向上依次递增。

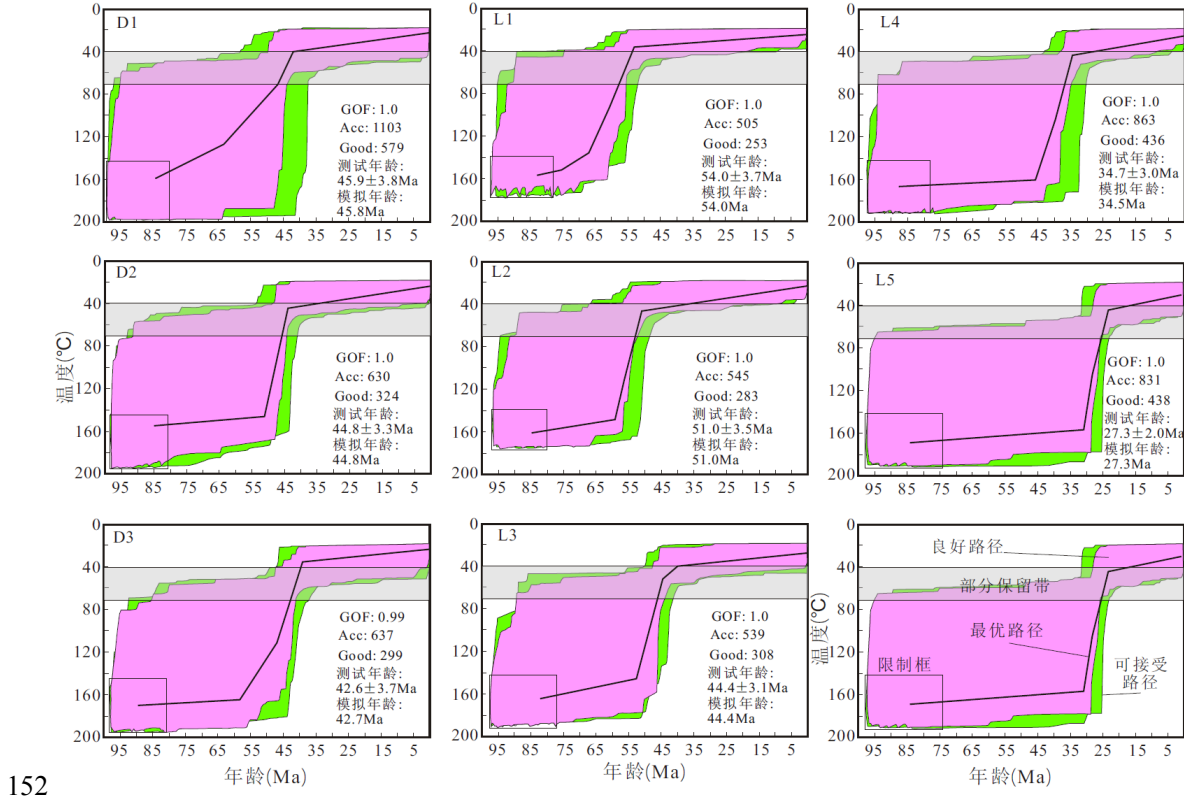


146 图 4 年龄-高程关系图，(a)多福山剖面；(b)锯齿山剖面

147 Fig. 4 Age-elevation relationship diagram, (a) Duofu Mountain profile; (b) Juchi Mountain profile

148 3.3 热历史反演结果

149 图 5 展示了多福山 3 个和锯齿山 5 个样品的单颗粒模拟结果，每个样品均显示了单一的冷
 150 却历史，多福山样品在 45.8-42.7 Ma，锯齿山上部 3 个样品在 54.0-44.4 Ma，底部 2 个样品在
 151 34.7-27.3 Ma 快速通过部分保留带。2 个剖面的单颗粒模拟年龄结果与实测数据结果一致。



152

153 图 5 多福山(D1-D3)和锯齿山(L1-L5)单颗粒磷灰石(U-Th)/He 年龄模拟结果
 154 Fig. 5 The modeled thermal histories of samples from Duofu (D1-D3) and Juchi (L1-L5) Mountains.
 155

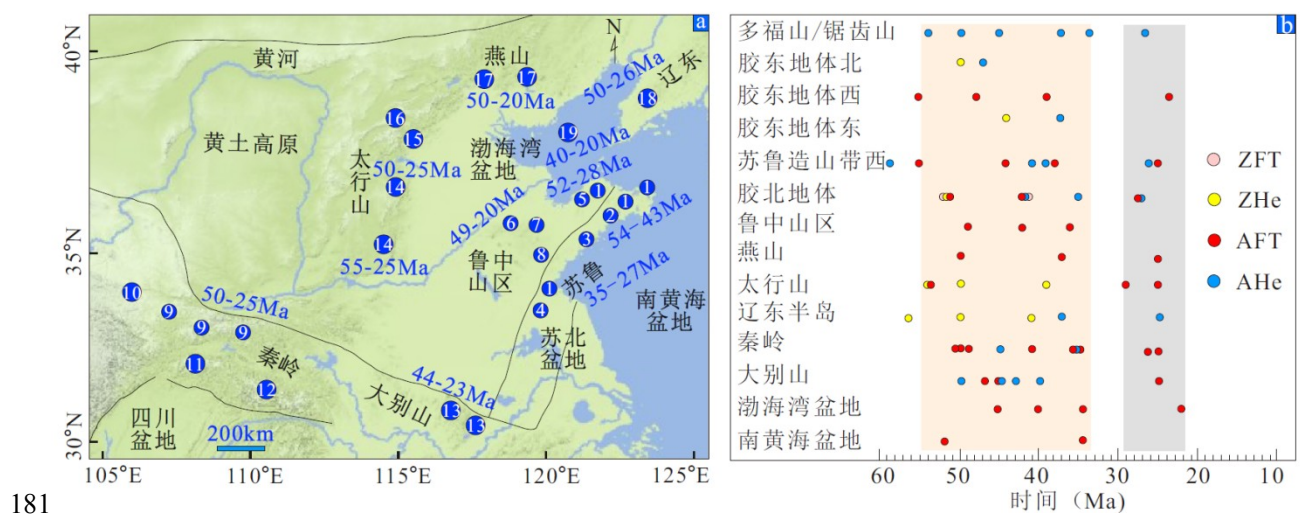
1564 讨论

1574.1 苏鲁造山带东段新生代两阶段剥露过程

158 年龄-高程对应关系和热历史模拟结果表明，多福山和锯齿山在早-中始新世(54-43 Ma)和
 159 渐新世(35-27 Ma)出现两阶段剥露过程。锆石和磷灰石(U-Th)/He 年龄，揭示胶东地体北部烟台、
 160 威海附近的岩体在 50-47 Ma 发生冷却抬升(Wu et al., 2016, 2017, 图 6a)。磷灰石 FT 年龄表明海
 161 阳北部和乳山北部岩体在 48-24 Ma 和 39 Ma 出现剥露过程(Zhao et al., 2018)。胶东地体东部荣
 162 成和石岛附近的岩体在 44 Ma(Wu et al., 2016)和 39 Ma 发生剥露(Siebel et al., 2009)。青岛附近
 163 的崂山岩体在 55 Ma 发生剥露(胡圣标等, 2005)。因而，苏鲁造山带东段在始新世和渐新世经历
 164 了广泛的剥露过程，其南北剥露时间具有时空同步性。磷灰石 FT 年龄记录了苏鲁造山带西段
 165 东海附近岩体在新生代早-中始新世(55-44 Ma)和渐新世(38-25 Ma)发生剥露(陈安定等, 2004;
 166 Liu et al., 2009)。Wu 等(2016)对日照和东海附近中生代花岗岩岩体开展磷灰石(U-Th)/He 年龄

167分析，表明新生代剥露事件分别发生在 59-41 Ma 和 39-26 Ma。这说明苏鲁造山带在这个时间
168内出现整体抬升过程。

169 从更大的范围来看，锆石和磷灰石低温热年代学结果(Deng et al., 2015; Wu et al., 2016; Liu
170 et al., 2017; Sun et al., 2017; Zhao et al., 2017)，指示了胶北地体新生代剥露主要发生在早-中始
171 新世(52-41 Ma)和渐新世(35-28 Ma)。鲁中山区在 49-42 Ma 和 36-20 Ma 发生剥露(唐智博等,
172 2011; 许立青等, 2016; 李理等, 2018)。碎屑磷灰石 FT 年龄揭示渤海湾盆地的沉积地层在 45-40
173 Ma 和 34-20 Ma 经历了挤压抬升过程(Chang et al., 2018; Xu et al., 2020)，同时其西部的太行山
174 在 55-40 Ma 和 30-25 Ma 发生剥露(Cao et al., 2015; Chang et al., 2019; Wu et al., 2020; Clinkscales
175 et al., 2021; Su et al., 2021; Zhang et al., 2021)。碎屑磷灰石 FT 年龄记录了南黄海盆地在 52 Ma
176 和 38 Ma 发生地层抬升剥蚀事件(庞玉茂等, 2018; Pang et al., 2019)。同期构造事件也发生在燕
177 山(吴中海和吴珍汉, 2003)、辽东半岛(Wang et al., 2018)、秦岭(Liu et al., 2013; Wang et al., 2013;
178 Chen et al., 2015; Yang et al., 2017; Zhang et al., 2020)和大别山(Grimmer et al., 2002; Reiners et al.,
179 2003; Hu et al., 2006; 周祖翼, 2015; Ding et al., 2021)。这说明在新生代早期中国东部普遍经历了
180 两阶段抬升过程(图 6b)。



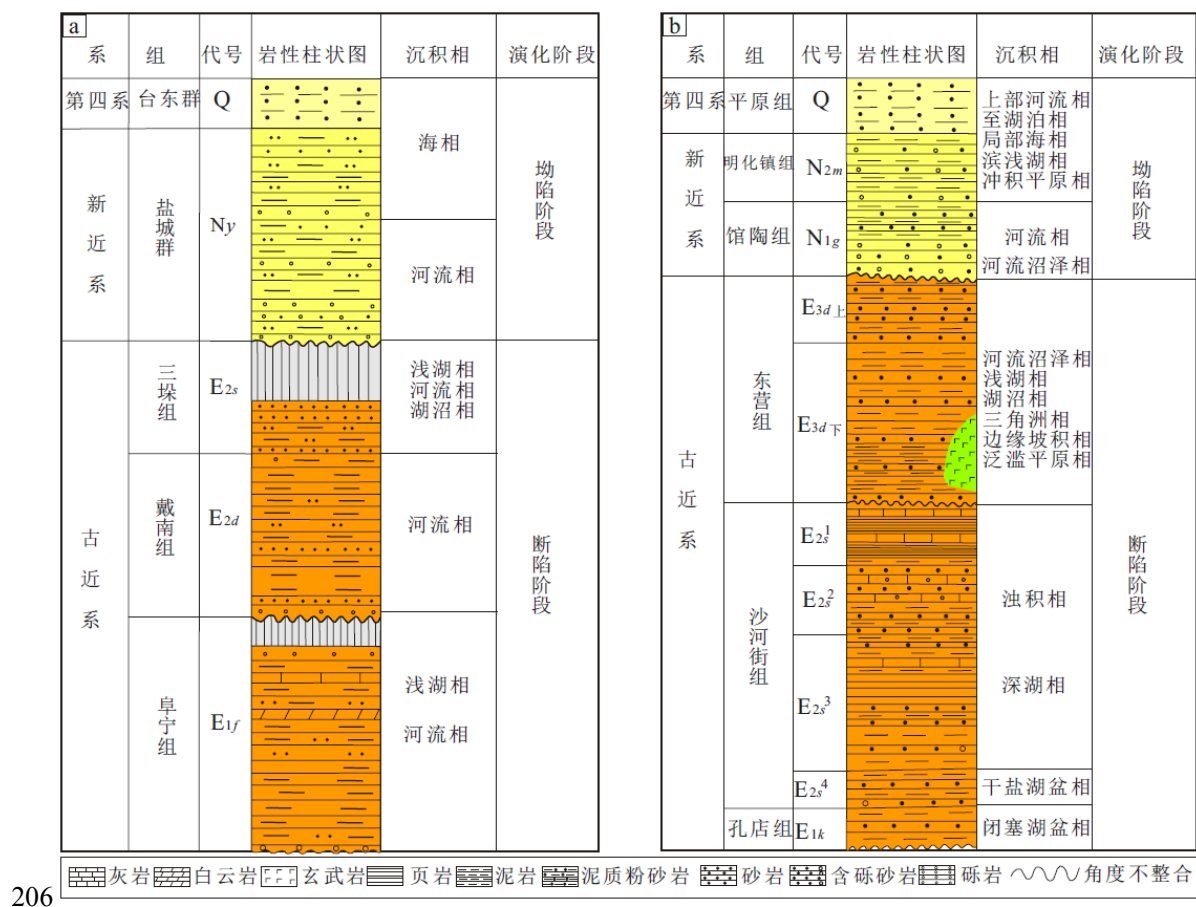
182 图 6 苏鲁造山带及其邻近区域早新生代构造隆升事件位置分布图(a)和时间汇总图(b)，图 a 中
183 数字代表研究位置：(1) Wu et al.(2016); (2) Zhao et al.(2018); (3) 胡圣标等(2005); (4) Liu et al.
184 (2009); (5) Liu et al.(2009); (6) 唐智博等(2011); (7) 李理等(2018); (8) 许立青等(2016); (9) Liu et al.
185 (2013); (10) Wang et al.(2013); (11) Zhang et al.(2020); (12) Yang et al.(2017); (13) Hu et al.(2006);
186 (14) Cao et al.(2015), Chang et al.(2019), Zhang et al.(2021); (15) Wu et al.(2020); (16) Clinkscales et
187 al.(2021); (17) 吴中海和吴珍汉(2003); (18) Wang et al.(2018); (19) Chang et al.(2018), Xu et al.
188 (2020)

189 Fig. 6 Distribution map of available exhumation ages (a) and time summary diagram (b) of early

190Cenozoic tectonic uplift events in the Sulu orogenic belt and adjacent areas. The numbers in blue
191circles indicate the position of referenced works.

1924.2 苏鲁造山带新生代隆升与邻区盆地的耦合关系

193 造山带隆升(地表相对于大地水准面或平均海平面的位移)产生的碎屑沉积物被搬运至邻近
194盆地，因而这些保存于沉积盆地的碎屑沉积物的沉积学和地层变形信息可用于恢复造山带的隆
195升过程(Chang et al., 2018; 林旭和刘静, 2019; Zhu et al., 2020)。碎屑锆石 U-Pb 年龄和重矿物物
196源示踪结果表明，南黄海盆地北部始新统地层(55-38 Ma)的碎屑物质主要来自胶东地体(Zhu et
197al., 2020)。碎屑锆石 U-Pb 年龄、重矿物和砂岩组分分析，说明苏北盆地(张妮, 2012)和南黄海
198盆地南部(Zhu et al., 2020)始新统地层的物质主要来自苏鲁造山带西段。结合苏北盆地(舒良树
199等, 2005; 邱燕等, 2016)和南黄海盆地(陈亮等, 2008)的地层在 55-50 Ma 和 38-25 Ma 分别出现角
200度不整合，并缺失部分地层(邱燕等, 2016, 图 7a)，说明此时区域发生构造变形事件。物源示踪
201结果结合地层的沉积时代表明，胶北地体(Sun et al., 2020)、鲁中山区(Liu et al., 2020)、太行山
202(Chen et al., 2020)和燕山(Tan et al., 2018; Liu et al., 2019)在早-中始新世和渐新世向渤海湾盆地
203提供碎屑物质，同时在盆地内沉积地层出现角度不整合、底砾岩(邱燕等, 2016; Chang et al.,
2042018)(图 7a)，说明这些碎屑物质的输入可主要归结为造山带的隆升剥蚀。所以，从盆地沉积
205学的角度也佐证了苏鲁造山带及其邻近区域在早-中始新世和晚渐新世发生构造变形事件。



206

207图 7 渤海湾盆地和南黄海盆地沉积柱状图(修改自邱燕等, 2016)

208Fig. 7 Synthetic sedimentary columns of the Bohai Bay Basin and South Yellow Sea Basin (Modified
209from Qiu et al., 2016)

210

211 苏鲁造山带早-中始新世和晚渐新世剥露过程与周缘板块活动时间相吻合。Northrup 等
212(1995)认为太平洋板块向西俯冲在中国东部造山带、盆地构造演化中起主导作用。早-中始新世
213(50-43 Ma)西太平洋板块以 NNW 向俯冲到欧亚大陆下部(Tarduno, 2007; Yin, 2010; Li et al.,
2142015; Zhu and Xu et al., 2019), 俯冲速率由晚白垩纪的 140-120 mm/a 下降到 40-30
215mm/a(Northrup et al., 1995; 包汉勇等, 2008; Liang and Wang, 2019), 此时西太平洋板块发生俯冲
216回撤, 中国东部处于伸展拉张环境, 在此构造背景下出现软流圈上涌、岩石圈拆沉(Yin, 2010;
217Li et al., 2015), 驱动苏鲁造山带发生构造抬升(Hu et al., 2006; Wu et al., 2016; Ding et al.,
2182021), 其周围出现南黄海、渤海湾等大型断陷盆地(Ren et al., 2002; Su et al., 2014a; Suo et al.,
2192014), 中国东部造山带与盆地的这一差异升降导致盆山地貌开始分异。受盆地断陷过程的影
220响, 这些沉积中心此时彼此分隔, 未形成统一的沉积分布区(图 1c, 图 6a)。进入晚渐新世(32-
22123 Ma), 太平洋板块向欧亚大陆俯冲的速率维持在 95-70 mm/a(Northrup et al., 1995; 包汉勇等,

222 2008; Liang and Wang, 2019), 俯冲方向转变为 NWW(Li et al., 2015), 中国东部伸展拉张环境逐
223 渐减弱, 开始以构造挤压背景为主(Ren et al., 2002; Su et al., 2014b), 这促使苏鲁造山带、鲁中
224 山区、太行山和燕山山脉内部基岩遭受新一期剥露, 邻近的南黄海、渤海湾等盆地发生地层缺
225 失或构造变形, 上述造山带隆升-剥露产生的碎屑物质进入南黄海盆地和渤海湾盆地后, 导致
226 后者开始进入坳陷演化阶段, 盆山耦合关系进一步加强, 从而奠定了中国东部盆-山地貌分布
227 格局的雏形(图 6b)。

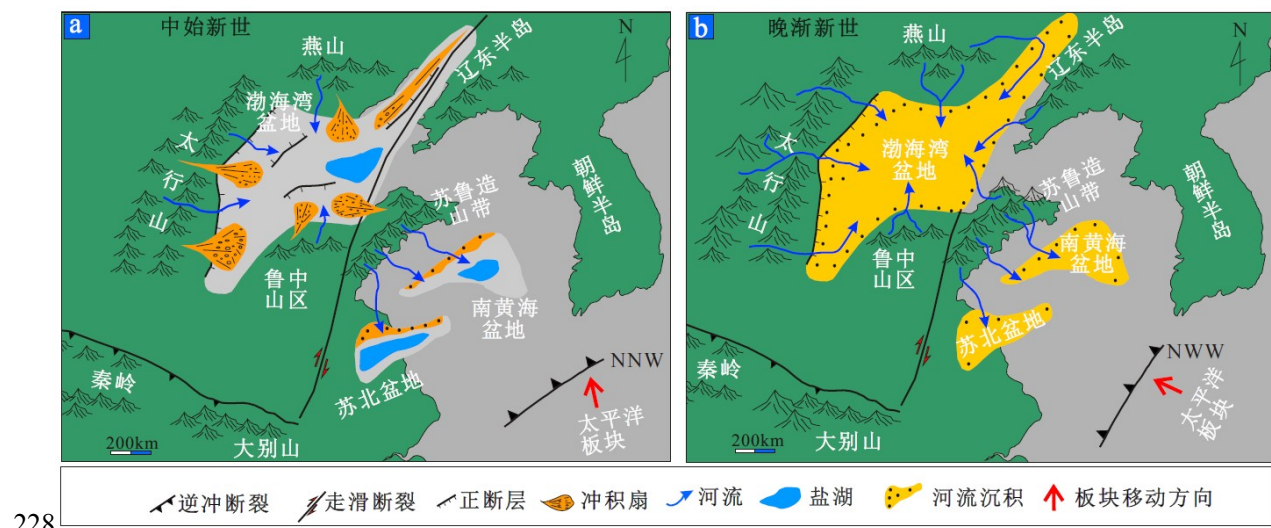


图 7 早新生代中国东部盆地分布复原图

230 Fig. 7 Palaeogeographic maps showing the distribution of basins and mountains in eastern China
 231 during the early Cenozoic. Note that maps are drawn using a present-day coastline.

2326 结论

233 本文利用磷灰石(U-Th)/He 热年代学方法约束苏鲁造山带东段南部的多福山和锯齿山的剥
234 露时间，得到如下结论：

235(1) 年龄-高程对应关系和热历史模拟结果表明多福山和锯齿山在早-中始新世(54-43 Ma)和渐新世(35-27 Ma)发生剥露。苏鲁造山带东段的南、北部在新生代的剥露时间基本一致；
236(2) 综合苏鲁造山带西段的低温热年代学，邻近南黄海盆地和渤海湾盆地沉积地层出现角度不整合，说明苏鲁造山带在早-中始新世和晚渐新世发生阶段性整体剥露。

239(3) 苏鲁造山带及其邻近地区在新生代早期的剥露过程，主要受控于西太平洋板块向欧亚大陆
240俯冲的影响，自新生代早期以来至少存在两期显著的盆山差异升降过程，从而奠定中国东部盆
241山分布格局。

242

243致谢：衷心

- 245Bao, H. Y., Guo, Zh. F., Zhang, L. L., et al. 2013. Tectonic dynamics of eastern China since the
246 formation of the Pacific plate. *Advances in Earth Science*, 28(3), 337-346 (in Chinese with
247 English abstract).
- 248Cao, X., Li, S., Xu, L., et al. 2015. Mesozoic-Cenozoic evolution and mechanism of tectonic
249 geomorphology in the central North China Block: constraint from apatite fission track
250 thermochronology. *Journal of Asian Earth Sciences*, 114, 41-53.
251 <https://doi:10.1016/j.jseaes.2015.03.041>.
- 252Cao, K., Leloup, P. H., Wang, G., et al. 2021. Thrusting, exhumation, and basin fill on the western
253 margin of the South China block during the India-Asia collision. *GSA Bulletin*, 133(1-2), 74-
254 90. <https://doi:10.1130/B35349.1>.
- 255Clinkscales, C., Kapp, P., Thomson, S., et al. 2021. Regional Exhumation and Tectonic History of the
256 Shanxi Rift and Taihangshan, North China. *Tectonics*, in
257 press. <https://doi.org/10.1029/2020TC006416>.
- 258Chang, J., Qiu, N., Zhao, X., et al. 2018. Mesozoic and Cenozoic tectono-thermal reconstruction of
259 the western Bohai Bay Basin (East China) with implications for hydrocarbon generation and
260 migration. *Journal of Asian Earth Sciences*, 160, 380-395.
261 <https://doi:10.1016/j.jseaes.2017.09.008>.
- 262Chang, J., Qiu, N., Liu, S., et al. 2019. Post-Triassic multiple exhumation of the Taihang Mountains
263 revealed via low-T thermochronology: implications for the paleo-geomorphologic
264 reconstruction of the North China Craton. *Gondwana Research*, 68, 34-49. <https://doi:10.1016/j.gr.2018.11.007>.
- 266Chen, A. D., Guo, T. L., Wan, J. L. 2004. Study on the tectonic uplift of the peripheral upheaval in
267 Jiangsu and Anhui by using fission track and isotopes dating methods. *Geotectonicaet
268 Metallogenica*, 28(4), 379-387(in Chinese with English abstract).
- 269Chen, L., Liu, Zh. H., Jin, Q. H. et al. 2008. Meso-Cenozoic tectonic evolution of the east depression
270 of North Yellow Sea. *Geotectonicaet Metallogenica*, 32(18), 308-316 (in Chinese with English
271 abstract).
- 272Chen, H., Hu, J., Wu, G., et al. 2015. Apatite fission-track thermochronological constraints on the
273 pattern of late Mesozoic-Cenozoic uplift and exhumation of the Qinling Orogen, central
274 China. *Journal of Asian Earth Sciences*, 114, 649-673.
275 <https://doi:10.1016/j.jseaes.2014.10.004>.
- 276Chen, H., Zhu, X., Wood, L. J., et al. 2020. Evolution of drainage, sediment-flux and fluvio-deltaic
277 sedimentary systems response in hanging wall depocentres in evolving non-marine rift basins:
278 Paleogene of Raoyang Sag, Bohai Bay Basin, China. *Basin Research*, 32(1), 116-145.
279 <https://doi:10.1111/bre.12371>.
- 280China Geological Survey. 2004. Geological map of the People's Republic of China (1:2.5 million).
281 Beijing: China map publishing house: 1. (in Chinese)
- 282Ding, R., Chang, Y., Min, K., et al. 2021. Post-orogenic topographic evolution of the Dabie orogen,
283 Eastern China: Insights from apatite and zircon (U-Th)/He
284 thermochronology. *Geomorphology*, 374, 107487. <https://doi:10.1016/j.geomorph.2020.107487>.
- 286Deng, B., Liu, S. G., Li, Z. W., et al. 2013. Differential exhumation at eastern margin of the Tibetan
287 Plateau, from apatite fission-track thermochronology. *Tectonophysics*, 591, 98-115.

- 288 https://doi:10.1016/j.tecto.2012.11.012.
- 289Deng, J., Wang, C., Bagas, L., et al. 2015. Cretaceous-Cenozoic tectonic history of the Jiaojia Fault
290 and gold mineralization in the Jiaodong Peninsula, China: constraints from zircon U-Pb, illite
291 K-Ar, and apatite fission track thermochronometry. *Mineralium Deposita*, 50(8), 987-1006.
292 https://doi:10.1007/s00126-015-0584-1.
- 293Flowers, R. M., Ketcham, R. A., Shuster, D. L., et al. 2009. Apatite (U-Th)/He thermochronometry
294 using a radiation damage accumulation and annealing model. *Geochimica et Cosmochimica
295 acta*, 73(8), 2347-2365. https://doi:10.1016/j.gca.2009.01.015.
- 296Gautheron, C., Tassan-Got, L., Barbarand, J., et al. 2009. Effect of alpha-damage annealing on apatite
297 (U-Th)/He thermochronology. *Chemical Geology*, 266(3-4), 157-170. https://
298 doi:10.1016/j.chemgeo.2009.06.001.
- 299Ge, Y., Liu-Zeng, J., Zhang, J., et al. 2020. Spatio-temporal variation in rock exhumation linked to
300 large-scale shear zones in the southeastern Tibetan Plateau. *Science China Earth
301 Sciences*, 63(4), 512-532. https://doi:10.1007/s11430-019-9567-y.
- 302Grimmer, J. C., Jonckheere, R., Enkelmann, E., et al. 2002. Cretaceous-Cenozoic history of the
303 southern Tan-Lu fault zone: apatite fission-track and structural constraints from the Dabie Shan
304 (eastern China). *Tectonophysics*, 359(3-4), 225-253. https://doi:10.1016/s0040-1951(02)00513-
305 9.
- 306Guo, J. H., Chen, F. Kun., Zhang, X. M. et al. 2005. Evolution of syn- to post-collisional magmatism
307 from north Sulu UHP belt, eastern China: zircon U-Pb geochronology. *Acta Petrologica
308 Sinica*, 21(4), 1281-1301(in Chinese with English abstract).
- 309Hu, Sh. B., Hao, J., Fu, M. X. et al. 2005. Cenozoic denudation and cooling history of Qinling-Dabie-
310 Sulu orogens: apatite fission track thermochronology constrains. *Acta Petrologica Sinica*,
311 21(4), 1167-1173(in Chinese with English abstract).
- 312Hu, S., Kohn, B. P., Raza, A., et al. 2006. Cretaceous and Cenozoic cooling history across the
313 ultrahigh pressure Tongbai-Dabie belt, central China, from apatite fission-track
314 thermochronology. *Tectonophysics*, 420(3-4), 409-429. https://doi:10.1016/j.tecto.2006.03.027.
- 315Jolivet, M., Dominguez, S., Charreau, J., Chen, Y., Li, Y., Wang, Q. 2010. Mesozoic and Cenozoic
316 tectonic history of the central Chinese Tian Shan: reactivated tectonic structures and active
317 deformation. *Tectonics*, 29(6), 1-30. https://doi.org/10.1029/2010TC002712.
- 318Ketcham, R. A. 2005. Forward and inverse modeling of low-temperature thermochronometry
319 data. *Reviews in mineralogy and geochemistry*, 58(1), 275-314.
320 https://doi:10.2138/rmg.2005.58.11.
- 321Li, L., Zhong, D. L., Chen, X. F. et al. 2018. Characteristics of NW-trending faults and evidence of
322 fission track in the Luxi Block. *Acta Geologica Sinica*, 92(3), 413-436 (in Chinese with
323 English abstract).
- 324Li, Z. D., Yu, X. F., Wang, Q. M. et al. 2018. Petrogenesis of Sanfoshan granite, Jiaodong: Diagenetic
325 physical and chemical condition, zircon U-Pb geochronology and Sr-Nd isotope constraints.
326 *Acta Petrologica Sinica*, 34(2), 447-468(in Chinese with English abstract).
- 327Li, S., Guo, L., Xu, L., et al. 2015. Coupling and transition of Meso-Cenozoic intracontinental
328 deformation between the Taihang and Qinling Mountains. *Journal of Asian Earth
329 Sciences*, 114, 188-202. http://dx.doi.org/10.1016/j.jseas.2015.04.011.
- 330Li, S., Suo, Y., Li, X., et al. 2019. Mesozoic tectono-magmatic response in the East Asian ocean-

- 331 continent connection zone to subduction of the Paleo-Pacific Plate. *Earth-Science*
332 *Reviews*, 192, 91-137. <https://doi:10.1016/j.earscirev.2019.03.003>.
- 333 Liang, J., Wang, H. 2019. Cenozoic tectonic evolution of the East China Sea Shelf Basin and its
334 coupling relationships with the Pacific Plate subduction. *Journal of Asian Earth Sciences*, 171,
335 376-387. <https://doi.org/10.1016/j.jseaes.2018.08.030>.
- 336 Lin, X., Liu, J. 2019. A review of mountain-basin coupling of Jianghan and Dongting basins with their
337 surrounding mountains. *Seismology and Geology*, 41(2), 499-520(in Chinese with English
338 abstract).
- 339 Liu, S. S., Weber, U., Glasmacher, U. A., et al. 2009. Fission track analysis and thermotectonic history
340 of the main borehole of the Chinese Continental Scientific Drilling
341 project. *Tectonophysics*, 475(2), 318-326. <https://doi:10.1016/j.tecto.2009.03.015>.
- 342 Liu, J., Zhang, P., Lease, R. O., et al. 2013. Eocene onset and late Miocene acceleration of Cenozoic
343 intracontinental extension in the North Qinling range-Weihe graben: Insights from apatite
344 fission track thermochronology. *Tectonophysics*, 584, 281-296.
345 <https://doi:10.1016/j.tecto.2012.01.025>.
- 346 Liu, X., Fan, H. R., Evans, N. J., et al. 2017. Exhumation history of the Sanshandao Au deposit,
347 Jiaodong: constraints from structural analysis and (U-Th)/He thermochronology. *Scientific
348 reports*, 7(1), 1-12. <https://doi:10.1038/s41598-017-08103-w>.
- 349 Liu, Q., Zhu, X., Zeng, H., et al. 2019. Source-to-sink analysis in an Eocene rifted lacustrine basin
350 margin of western Shaleitian Uplift area, offshore Bohai Bay Basin, eastern China. *Marine
351 and Petroleum Geology*, 107, 41-58. <https://doi:10.1016/j.marpetgeo.2019.05.013>.
- 352 Liu, H., van Loon, A. T., Xu, J., et al. 2020. Relationships between tectonic activity and sedimentary
353 source-to-sink system parameters in a lacustrine rift basin: A quantitative case study of the
354 Huanghekou Depression (Bohai Bay Basin, E China). *Basin Research*, 32(4), 587-612. <https://doi:10.1111/bre.12374>.
- 356 Liu-Zeng, J., Zhang, J., McPhillips, D., et al. 2018. Multiple episodes of fast exhumation since
357 Cretaceous in southeast Tibet, revealed by low-temperature thermochronology. *Earth and
358 Planetary Science Letters*, 490, 62-76. <https://doi:10.1016/j.epsl.2018.03.011>.
- 359 Northrup, C. J., Royden, L. H., Burchfiel, B. C. 1995. Motion of the Pacific plate relative to Eurasia
360 and its potential relation to Cenozoic extension along the eastern margin of
361 Eurasia. *Geology*, 23(8), 719-722.
362 [https://doi.org/10.1130/0091-7613\(1995\)023<0719:MOTPPR>2.3.CO;2](https://doi.org/10.1130/0091-7613(1995)023<0719:MOTPPR>2.3.CO;2).
- 363 Pang, Y., Guo, X., Han, Z., et al. 2018. Analysis of apatite fission track of strata denudation since Late
364 Cretaceous in the central uplift of South Yellow Sea. *Earth Science*, 43(6), 1921-1930(in
365 Chinese with English abstract).
- 366 Pang, Y. M., Guo, X. W., Han, Z. Z., et al. 2019. Mesozoic-Cenozoic denudation and thermal history
367 in the Central Uplift of the South Yellow Sea basin and the implications for hydrocarbon
368 systems: Constraints from the CSDP-2 borehole. *Marine and Petroleum Geology*, 99, 355-369.
- 369 Qiu, Y., Wang, L. F., Huang, W. K. 2016. The Mesozoic and Cenozoic Sedimentary Basins in the Sea
370 Area of China. *Geological Publishing House*, Beijing, 1-233(in Chinese with English abstract).
- 371 Ren, J., Tamaki, K., Li, S., et al. 2002. Late Mesozoic and Cenozoic rifting and its dynamic setting in
372 Eastern China and adjacent areas. *Tectonophysics*, 344(3-4), 175-205. [https://doi.org/10.1016/S0040-1951\(01\)00271-2](https://doi.org/10.1016/S0040-1951(01)00271-2).

- 374 Reiners, P. W., Zhou, Z., Ehlers, T. A., et al. 2003. Post-orogenic evolution of the Dabie Shan, eastern
375 China, from (U-Th)/He and fission-track thermochronology. *American Journal of*
376 *Science*, 303(6), 489-518. <https://doi:10.2475/ajs.303.6.489>.
- 377 Regional geology of Shandong province. Geological Publishing House, Beijing, 1-595(in Chinese
378 with English abstract).
- 379 Regional geological map of Rushan 1:200000. Beijing: China Cartographic Publishing House, 1(in
380 Chinese).
- 381 Siebel, W., Danišík, M., Chen, F. 2009. From emplacement to unroofing: thermal history of the
382 Jiazhishan gabbro, Sulu UHP terrane, China. *Mineralogy and Petrology*, 96(3-4), 163-
383 175. <https://doi:10.1007/s00710-009-0058-1>.
- 384 Su, J., Zhu, W., Chen, J., et al. 2014a. Wide rift model in Bohai Bay Basin: Insight into the destruction
385 of the North China Craton. *International Geology Review*, 56(5), 537-554.
386 <http://www.tandfonline.com/loi/tigr20>.
- 387 Su, J., Zhu, W., Chen, J., et al. 2014b. Cenozoic inversion of the East China Sea Shelf Basin:
388 implications for reconstructing Cenozoic tectonics of eastern China. *International Geology
389 Review*, 56(12), 1541-1555. <https://doi.org/10.1080/00206814.2014.951004>.
- 390 Su, P., He, H., Tan, X., Liu, Y., Shi, F., Kirby, E. 2021. Initiation and Evolution of the Shanxi Rift
391 System in North China: Evidence From Low-Temperature Thermochronology in a Plate
392 Reconstruction Framework. *Tectonics*, 40(3), e2020TC006298.
393 <https://doi.org/10.1029/2020TC006298>.
- 394 Suo, Y., Li, S., Yu, S., et al. 2014. Cenozoic tectonic jumping and implications for hydrocarbon
395 accumulation in basins in the East Asia Continental Margin: *Journal of Asian Earth Sciences*,
396 88, 28-40. doi:10.1016/j.jseaes.2014.02.019.
- 397 Sun, H., Li, H., Liu, L., et al. 2017. Exhumation history of the Jiaodong and its adjacent areas since
398 the Late Cretaceous: Constraints from low temperature thermochronology. *Science China: Earth
399 Sciences*, 60(3), 531-545. <https://doi:10.1007/s11430-016-0021-1>.
- 400 Sun, Z., Zhu, H., Xu, C., et al. 2020. Reconstructing provenance interaction of multiple sediment
401 sources in continental down-warped lacustrine basins: An example from the Bodong area,
402 Bohai Bay Basin, China. *Marine and Petroleum Geology*, 113, 104142.
403 <https://doi:10.1016/j.marpetgeo.2019.104142>.
- 404 Shen, X., Tian, Y., Li, D., et al. 2016. Oligocene-Early Miocene river incision near the first bend of the
405 Yangze River: Insights from apatite (U-Th-Sm)/He thermochronology. *Tectonophysics*, 687, 223-
406 231. <https://doi.org/10.1016/j.tecto.2016.08.006>.
- 407 Shu, L. Sh., Wang, B. Wang., L. Sh., et al. 2005. Analysis of Northern Jiangsu prototype basin from
408 Late Cretaceous to Neogene. *Geological Journal of China Universities*, 11(4), 534-543(in
409 Chinese with English abstract).
- 410 Shuster, D. L., Flowers, R. M., Farley, K. A. 2006. The influence of natural radiation damage on
411 helium diffusion kinetics in apatite. *Earth and Planetary Science Letters*, 249(3-4), 148-161.
412 <https://doi.org/10.1016/j.epsl.2006.07.028>.
- 413 Tan, M., Zhu, X., Liu, W., et al. 2018. Sediment routing systems in the second member of the Eocene
414 Shahejie Formation in the Liaoxi Sag, offshore Bohai Bay Basin: A synthesis from tectono-
415 sedimentary and detrital zircon geochronological constraints. *Marine and Petroleum
416 Geology*, 94, 95-113. <https://doi:10.1016/j.marpetgeo.2018.04.003>.

- 417 Tang, J., Zheng, Y. F., Wu, Y. B., et al. 2008. Zircon U-Pb age and geochemical constraints on the
418 tectonic affinity of the Jiaodong terrane in the Sulu orogen, China. *Precambrian*
419 *Research*, 161(3-4), 389-418. <https://doi.org/10.1016/j.precamres.2007.09.008>.
- 420 Tang, Zh. B., Li, L. Shi, M. X. et al. 2011. Fission track thermochronology of Late Cretaceous -
421 Cenozoic uplifting events of the Mengshan Mountain in the Western Shandong Rise, China.
422 *Acta Scientiarum Naturalium Universitatis Sunyatseni*, 50(2), 127-133 (in Chinese with
423 English abstract).
- 424 Tarduno, J. A. 2007. On the motion of Hawaii and other mantle plumes. *Chemical Geology*, 241(3-4),
425 234-247. <https://doi:10.1016/j.chemgeo.2007.01.021>.
- 426 Vermeesch, P. 2010. HelioPlot, and the treatment of overdispersed (U-Th-Sm)/He data. *Chemical*
427 *Geology*, 271(3-4), 108-111. <https://doi:10.1016/j.chemgeo.2010.01.002>.
- 428 Wang, X., Zattin, M., Li, J., et al. 2013. Cenozoic tectonic uplift history of western Qinling: evidence
429 from sedimentary and fission-track data. *Journal of Earth Science*, 24(4), 491-505.
430 <https://doi:10.1007/s12583-013-0345-y>.
- 431 Wang, Y., Wang, F., Wu, L., et al. 2018. (U-Th)/He thermochronology of metallic ore deposits in the
432 Liaodong Peninsula: Implications for orefield evolution in northeast China. *Ore Geology*
433 *Reviews*, 92, 348-365. <https://doi.org/10.1016/j.oregeorev.2017.11.025>.
- 434 Wu, Zh. H., Wu, Zh. H. 2003. Low-temperature thermochronological analysis of the uplift history of
435 the Yanshan Mountain and its neighboring area. *Acta Geologica Sinica*, 77(3), 399-406 (in
436 Chinese with English abstract).
- 437 Wu, Y. B., Zheng, Y. F. 2013. Tectonic evolution of a composite collision orogen: an overview on the
438 Qinling-Tongbai-Hong'an-Dabie-Sulu orogenic belt in central China. *Gondwana*
439 *Research*, 23(4), 1402-1428. <https://doi:10.1016/j.gr.2012.09.007>.
- 440 Wu, L., Monié, P., Wang, F., et al. 2016. Cenozoic exhumation history of Sulu terrane: Implications
441 from (U-Th)/He thermochrology. *Tectonophysics*, 672, 1-15.
442 <https://doi:10.1016/j.tecto.2016.01.035>.
- 443 Wu, L., Monié, P., Wang, F., et al. 2017. Multi-phase cooling of Early Cretaceous granites on the
444 Jiaodong Peninsula, East China: evidence from $^{40}\text{Ar}/^{39}\text{Ar}$ and (U-Th)/He
445 thermochronology. *Journal of Asian Earth Sciences*, 160, 334-347.
446 <https://doi.org/10.1016/j.jseaes.2017.11.014>.
- 447 Wu, L., Shi, G., Danišík, M., et al. 2019. MK-1 Apatite: A New Potential Reference Material for (U-
448 Th)/He Dating. *Geostandards and Geoanalytical Research*, 43(2), 301-315.
449 <https://doi:10.1111/ggr.12258>.
- 450 Wu, L., Wang, F., Yang, J., et al. 2020. Meso-Cenozoic uplift of the Taihang Mountains, North China:
451 evidence from zircon and apatite thermochronology. *Geological Magazine*, 157(7), 1097-1111.
452 <https://doi:10.1017/S0016756819001377>.
- 453 Wu, L., Wang, F., Zhang, Z., et al. 2021. Reappraisal of the applicability of MK-1 apatite as a
454 reference standard for (U-Th)/He geochronology. *Chemical Geology*, 120255.
455 <https://doi.org/10.1016/j.chemgeo.2021.120255>.
- 456 Xu, L. Q., Li, S. Zh., Guo, L. L. et al. 2016. Impact of the Tan-Lu fault zone on uplift of the Luxi
457 Rise: Constraints from apatite fission track thermochronology. *Acta Petrologica Sinica*, 32(4),
458 1153-1170 (in Chinese with English abstract).
- 459 Xu, W., Qiu, N., Chang, J., et al. 2020. Mesozoic-Cenozoic thermal evolution of the Linqin Sub-

- 460 basin, Bohai Bay Basin (eastern North China Craton): Constraints from vitrinite reflectance
461 data and apatite fission track thermochronology. *Geological Journal*, 55(7), 5049-5061. <https://doi.org/10.1002/gj.3701>.
- 463 Yang, Q., Santosh, M., Shen, J. et al. 2014. Juvenile vs. recycled crust in NE China: Zircon U-Pb
464 geochronology, Hf isotope and an integrated model for Mesozoic gold mineralization in the
465 Jiaodong Peninsula. *Gondwana Research*, 25(4), 1445-1468.
466 <https://doi.org/10.1016/j.gr.2013.06.003>.
- 467 Yang, R., Fellin, M. G., Herman, F., et al. 2016. Spatial and temporal pattern of erosion in the Three
468 Rivers Region, southeastern Tibet. *Earth and Planetary Science Letters*, 433, 10-20.
469 <https://doi.org/10.1016/j.epsl.2015.10.032>.
- 470 Yang, Z., Shen, C., Ratschbacher, L., et al. 2017. Sichuan Basin and beyond: Eastward foreland
471 growth of the Tibetan Plateau from an integration of Late Cretaceous-Cenozoic fission track
472 and (U-Th)/He ages of the eastern Tibetan Plateau, Qinling, and Daba Shan. *Journal of*
473 *Geophysical Research: Solid Earth*, 122(6), 4712-4740.
474 <https://doi.org/10.1002/2016JB013751>.
- 475 Yin, A. 2010. Cenozoic tectonic evolution of Asia: A preliminary synthesis. *Tectonophysics*, 488(1-4),
476 293-325. <https://doi.org/10.1016/j.tecto.2009.06.002>.
- 477 Yu, J., Zheng, D., Pang, J., et al. 2019. Miocene Range Growth Along the Altyn Tagh Fault: Insights
478 From Apatite Fission Track and (U-Th)/He Thermochronometry in the Western Danghenan
479 Shan, China. *Journal of Geophysical Research: Solid Earth*, 124(8), 9433-9453.
480 <https://doi.org/10.1029/2019JB017570>.
- 481 Zhao, R., Wang, Q., Liu, X., et al. 2018. Uplift history of the Jiaodong Peninsula, eastern North China
482 Craton: implications for lithosphere thinning and gold mineralization. *Geological Magazine*, 155(4), 979-991. <https://doi.org/10.1017/S0016756816001254>.
- 484 Zhang, N. 2012. Comprehensive provenance study in sedimentary basin: an example from the
485 Paleogene Dainan Formation of Gaoyou Depression, the North Jiangsu Basin. *Nanjing University*, 1-138(in Chinese with English abstract).
- 487 Zhang, W. B., Wu, L., Wang, F. 2016. Factors impacting the accuracy of apatite(U-Th)/He dating.
488 *Seismology and Geology*, 38(4), 1107-1123(in Chinese with English abstract).
- 489 Zhang, Y. P., Zheng, W. J., Wang, W. T., et al. 2020. Rapid Eocene Exhumation of the West Qinling
490 Belt: Implications for the Growth of the Northeastern Tibetan Plateau. *Lithosphere*, 2020(1), 1-
491 12. <https://doi.org/10.2113/2020/8294751>.
- 492 Zhang, J., Wang, Y., Zhang, B., Qu, J., Li, J., Long, Y., Hui, J. 2021. Tectonothermal events in the
493 central North China Craton since the Mesozoic and their tectonic implications: Constraints
494 from low-temperature thermochronology. *Tectonophysics*, 228769.
495 <https://doi.org/10.1016/j.tecto.2021.228769>.
- 496 Zheng, Y. 2008. A perspective view on ultrahigh-pressure metamorphism and continental collision in
497 the Dabie-Sulu orogenic belt. *Chinese Science Bulletin*, 53(20), 3081-3104.
498 <https://doi.org/10.1007/s11434-008-0388-0>.
- 499 Zhou, Z. Y. 2015. Low temperature thermochronology: Principles and Applications. *Science Press*,
500 Beijing, 1-230 (in Chinese with English abstract).
- 501 Zhu, R., Xu, Y. 2019. The subduction of the west Pacific plate and the destruction of the North China
502 Craton. *Science China: Earth Sciences*, 62(9), 1340-1350. [https://doi.org/10.1007/s11430-018-](https://doi.org/10.1007/s11430-018-0)

- 503 9356-y.
- 504 Zhu, R. X., Zhu, G. Li, J. W. 2020. The North China Craton destruction. *Science Press*, 1-417 (in
505 Chinese with English abstract).
- 506 Zhu, X., Shen, C., Zhou, R., et al. 2020. Paleogene sediment provenance and paleogeographic
507 reconstruction of the South Yellow Sea Basin, East China: Constraints from detrital zircon U-
508 Pb geochronology and heavy mineral assemblages. *Palaeogeography, Palaeoclimatology,*
509 *Palaeoecology*, 553, 109776. <https://doi:10.1016/j.palaeo.2020.109776>.
- 510 包汉勇, 郭战峰, 张罗磊, 等. 2013. 太平洋板块形成以来的中国东部构造动力学背景. 地球科学进
511 展, 28(3), 337-346.
- 512 陈安定, 郭彤楼, 万景林. 2004. 裂变径迹、同位素年龄研究苏皖周边隆起构造抬升. 大地构造与
513 成矿学, 28(4), 379-387.
- 514 陈亮, 刘振湖, 金庆焕, 等. 2008. 北黄海盆地东部坳陷中新生代构造演化. 大地构造与成矿学,
515 32(18), 308-316.
- 516 郭敬辉, 陈福坤, 张晓曼, 等. 2005. 苏鲁超高压带北部中生代岩浆侵入活动与同碰撞-碰撞后构造
517 过程: 锆石 U-Pb 年代学. 岩石学报, 21(4), 1281-1301.
- 518 胡圣标, 郝杰, 付明希, 等. 2005. 秦岭-大别-苏鲁造山带白垩纪以来的抬升冷却史—低温年代学
519 数据约束. 岩石学报, 21(4), 1167-1173.
- 520 李理, 钟大赉, 陈霞飞, 等. 2018. 鲁西地块 NW 走向断层的活动特征及裂变径迹证据. 地质学报,
521 92(3), 413-436.
- 522 李增达, 于晓飞, 王全明, 等. 2018. 胶东三佛山花岗岩的成因: 成岩物理化学条件, 锆石 U-Pb 年
523 代学及 Sr-Nd 同位素约束. 岩石学报, 34(2), 447-468.
- 524 林旭, 刘静. 2019. 江汉和洞庭盆地与周缘造山带盆山耦合研究进展. 地震地质, 41(2), 499-520.
- 525 庞玉茂, 郭兴伟, 韩作振, 等. 2018. 南黄海中部隆起晚白垩世以来地层剥蚀的磷灰石裂变径迹分
526 析. 地球科学, 43(6), 1921-1930.
- 527 邱燕, 王立飞, 黄文凯. 2016. 中国海域中新生代沉积盆地. 地质出版社, 北京, 1-233.
- 528 乳山 1:20 万区域地质图. 北京: 中国地图出版社, 1.
- 529 山东省区域地质志. 地质出版社, 北京, 1-595.
- 530 舒良树, 王博, 王良书, 等. 2005. 苏北盆地晚白垩世-新近纪原型盆地分析. 高校地质学报, 11(4),
531 534-543.
- 532 唐智博, 李理, 时秀朋, 等. 2011. 鲁西隆起蒙山晚白垩世-新生代抬升的裂变径迹证据. 中山大学学
533 报(自然科学版), 50(2), 127-133.
- 534 吴中海, 吴珍汉. 2003. 燕山及邻区晚白垩世以来山脉隆升历史的低温热年代学证据. 地质学报,
535 77(3), 399-406.
- 536 许立青, 李三忠, 郭玲莉, 等. 2016. 郯庐断裂带对鲁西隆升过程的影响: 磷灰石裂变径迹证据. 岩
537 石学报, 32(4), 1153-1170.
- 538 张妮. 2012. 沉积盆地的物源综合研究-以苏北盆地高邮凹陷古近系戴南组为例. 南京大学, 1-138.
- 539 张炜斌, 吴林, 王非. 2016. 磷灰石(U-Th)/He 年龄准确度的影响因素. 地震地质, 38(4), 1107-1123.
- 540 中国地质调查局. 2004. 中华人民共和国地质图 1:250 万说明书. 北京: 中国地图出版社, 1.
- 541 周祖翼. 2015. 低温热年代学: 原理与应用. 科学出版社, 北京, 1-230.
- 542 朱日祥, 朱光, 李建威. 2020. 华北克拉通破坏. 科学出版社, 1-417.